ELSEVIER

Coordination Chemistry Reviews
178–180 (1998) 1019–1049

COORDINATION CHEMISTRY REVIEWS

From Lindqvist and Keggin ions to electronically inverse hosts: Ab initio modelling of the structure and reactivity of polyoxometalates

Marie-Madeleine Rohmer [a], Marc Bénard [a,*], Jean-Philippe Blaudeau [a], Juan-M. Maestre [b], Josep-M. Poblet [b]

[a] *Laboratoire de Chimie Quantique, UMR 7551, CNRS and Université Louis Pasteur, F-67000 Strasbourg, France*

[b] *Departament de Química Física Inorgánica, Universitat Rovira i Virgili, E-43005 Tarragona, Spain*

Received 19 December 1997; accepted 2 June 1998

Contents

Abstract

This review reports the ab initio Hartree–Fock and DFT calculations which have been carried out recently in our two groups in order to investigate the electronic structure of

* Corresponding author. Fax: +33 03 88612085; e-mail: benard@quantix.u-strasbg.fr

PII S0010-8545(98)00162-3

polyoxometalate clusters, either totally oxidized like $(V_{10}O_{28})^{6-}$ or partly reduced such as $[PMo_{12}O_{40}(VO)_2]^{5-}$. The approach of protons or cationic groups to the external coating of oxygen atoms and their preferred site of fixation can be predicted from the topology of the computed distribution of molecular electrostatic potentials (MEP). The MEP distribution can also be used to get a better understanding of the formation of inclusion and encapsulation complexes. Hemispherical carcerands like $(V_{12}O_{32})^{4-}$ develop a dipolar field in the accessible part of their cavity susceptible to attract small molecules with a permanent dipole like RCN ($R=CH_3$, C_6H_5). The "electronically inverse" host anions known to encapsulate anionic species are formed in solution by means of a template mechanism which tends to maximize the electrostatic potential at the place of the guest anion. A correlation is provided between the topology of the host and its MEP distribution which explains, from simple geometric considerations, the differences between electronically normal and electronically inverse hosts, and shows that the host cage tends to get adapted not only to the shape of the guest molecule, but also to its electrostatic potential distribution.

Keywords: Ab initio; Density functional theory; Electrostatic potentials; Encapsulation complexes; Host–guest complexes; Lattice potential; Polyoxometalates; Quantum chemistry

1. Introduction

Polyoxometallates containing octahedral, square pyramidal, or tetrahedral coordinated metal atoms often yield cage-like molecular anions with interesting structural and organizational properties. Some of those structures correspond to standard and recurrent conformations such as the Lindqvist ion $(M_6O_{19})^{n-}$ or the α-Keggin ion $(XM_{12}O_{40})^{n-}$ (X = B, P, As, Si, Cu, Fe, Co). Since the central ion, O^{2-} in Lindqvist structures, $(XO_4)^{m-}$ in Keggin ones, is perfectly inserted into the octahedral environment of metal atoms, those complexes are generally not considered as encapsulation compounds of the form $O^{2-}@(M_6O_{18})^{(n-2)-}$ or $(XO_4)^{m-}@(M_{12}O_{36})^{(n-m)-}$ as they could be, and have sometimes been described [1–4]. Obviously, borderline cases do exist such as the $[(VO_4)@(V_{18}O_{45})]^{9-}$ complex recently characterized by Suber et al. [5] and the "extended Keggin" structures encapsulating tetrahedral ions like $[(VO_4)@H_9V_{18}O_{42})]^{6-}$, $[(SO_4)@(V_{18}O_{42})]^{8-}$ [6] or $[(SO_4)@As_4Mo_6V_7O_{39})]^{4-}$ [7]. The clear identification of a polyoxoanion as a supramolecular species involving a host cage and an encapsulated guest therefore introduced a quite novel, unusual, and, at first, controversial concept [1]. This representation eventually gained recognition in view of the lability of the guest — or hostage — molecule in the host cage [8,9] and also due to the unprecedented template role of the encapsulated anion for controlling the organization, size and shape of the surrounding cluster shell [1,4].

Polyoxometalate hosts most often encapsulate charged species. An intuitive optimization of electrostatic interactions leads to consideration of the complex, in the crystal or in solution, as an onion-like structure composed of successive layers with opposite charges. The negatively charged polyoxometalate host should then require inside, the presence of a positively charged guest fragment, and outside, the stabilization induced by an appropriate shell of countercations. Complexes with such a

structure do indeed exist [10,11], and a number have been collected and described in a recent review [12]. More difficult to explain on electrostatic grounds are the complexes formed by template shaping of a polyoxometallate host around a neutral or negatively charged species [12]. Neutral guest molecules such as acetonitrile or benzonitrile have been shown to give stable associations with the bowl-shaped ion $(V_{12}O_{32})^{4-}$, both in the crystal and in solution [13–15]. Water could be characterized as a guest molecule [16–19] when the hydrothermal synthesis is carried out at high pH values ($\sim$14) [19]. Finally, an impressive series of polyoxometalate cages whose shape appears closely adapted to that of a negatively charged guest has led to the self-explanatory concept of "electronically inverse hosts" [12]. Even though the empirical knowledge acquired from monitoring those supramolecular assemblies has permitted us to gain some insight into the mechanisms involved [12,20,21], little effort has been devoted to modelling the formation of those molecules by the methods of quantum chemistry, mainly because of the large sizes of those supramolecular systems, and also because of the versatility of the metal oxide fragments which allows for a large number of structures to be obtained from the same species [22].

From the ab initio and DFT studies carried out in our two groups since the beginning of the present decade, we think, however, that it is now possible to answer some of the pending questions concerning the nature, reactivity and assembly mechanism of metal–oxide cage complexes. More specifically, we would like to review and discuss the calculations which have been carried out on some Lindqvist and Keggin structures, on Klemperer's inclusion complexes [13,14], as well as on electronically inverse host–guest systems, in order to address the following problems:

(i) Determination of the relative activities of the external oxygen sites with respect to protonation or more generally with respect to an electrophilic attack.

(ii) Localization vs. delocalization of the d electrons on the metal framework in reduced polyoxoanions.

(iii) Definition of a quantitative criterion to separate or not a cage complex into host and guest subsystems.

(iv) Discovering how the electronically inverse host–guest complexes overcome the electrostatic repulsion by taking advantage of the host topology.

2. Computed molecular electrostatic potentials (MEP)

Supramolecular chemistry and self-organization are generally assumed to be monitored by non-covalent interactions, namely by electrostatic attraction, van der Waals forces and hydrogen bonding, although a more flexible, extensive definition of the bonding has been advocated to approach inorganic host–guest chemistry [12]. The other aspect of polyoxometallate chemistry we are interested in, namely the approach of a proton, or of a cationic group, to the external coating of oxygen atoms, is also conditioned by electrostatic attraction, even though the fixation of the positively charged species induces some reorganization of the polyoxometalate structure [23].

For those reasons, we have proposed an approach to the local activity of a polyoxometalate site, either exohedral or endohedral, based upon the computed distribution of electrostatic potentials [24]. The MEP at a given point R_p of the molecular environment is defined as the energy acquired by a positive charge located at this point and undergoing the field generated by the molecule:

$$V(r)=\sum_{A}\frac{Z_A}{|r-R_A|}-\int\frac{\rho(r')}{|r-r'|}\,dr'$$

where Z_A represents the nuclear charge of atom A, and $p(r')$ corresponds to the molecular electron density functional, determined from an ab initio SCF wavefunction. The electrostatic potential is computed for planar or spherical cuts of the molecular space and represented in this latter case by means of a stereographic projection.

The topology of the MEP distribution in the accessible region of the molecule is expected to provide information concerning the approach of a reagent, either electrophilic, or dipolar, or, to some extent, nucleophilic. The electrophilic species, represented as a positive charge, will tend to minimize its potential energy by reaching — or approaching as much as possible — a minimum of the MEP distribution. The external faces of a polyoxometalate molecule will generate a large number of such minima, generally associated with a specific oxygen atom or with a basin composed of several oxygen atoms close together. According to the same logics, a negative charge should minimize its potential energy by approaching a maximum of the MEP distribution, but those maxima coincide with the atomic nuclei and are therefore inaccessible to a real nucleophilic agent. The accessible regions most favourable to a nucleophilic attack or, according to the logics of the template mechanism, the favourable regions created by the presence of a nucleophilic species should coincide with a high value of the electrostatic potential relative to neighbouring minima. In some cases, those regions can be characterized topologically by a saddle point of the MEP distribution.

3. The MEP distribution of Lindqvist ions

3.1. The decavanadate ion $(V_{10}O_{28})^{6-}$

The $(V_{10}O_{28})^{6-}$ ion is composed of two fused Lindqvist cages sharing a face composed of two vanadium and four oxygen atoms [Fig. 1(a)]. The external coating of oxygen atoms is characterized by four large surfaces composed each of nine close-packed atoms [Fig. 1(b)].

One of those atoms (site B) is surrounded by six nearest neighbours, an environment with no equivalent in single Lindqvist cages and reminiscent of the infinite surface. Decavanadate ions can undergo multiple protonations, and the preferred sites for proton fixation were determined from the changes observed in the ^{17}O NMR spectrum upon protonation [25]. A large shift was observed in

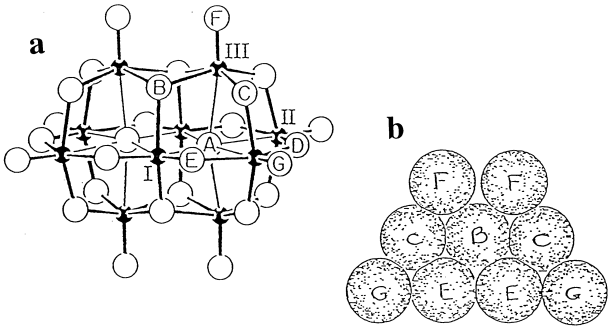

Fig. 1. (a) The decavanadate ion $(V_{10}O_{28})^{6-}$. The letters A to G represent the distinct oxygen sites. (b) The nine-atom oxygen array found on the surface of the dacavanadate ion. Reproduced from Ref. [23] with permission.

the NMR peak associated with site B, whereas site C was also affected by protonation. The crystallographic characterization of the triprotonated species $H_3V_{10}O_{28}[(C_6H_5)_4P]_3 \cdot 4CH_3CN$ [23] confirmed those results to some extent since the protons were assigned to one B site and to the neighbouring C sites. The position of the protons could, however, have been influenced by the possibility of obtaining a dimeric species stabilized by six hydrogen bonds [23] (Fig. 2).

As expected, the MEP distribution computed in the vicinity of the 26 external oxygen atoms of an isolated $[V_{10}O_{28}]^{6-}$ ion has a rather complex topology, characterized by 20 local minima. All oxygen atoms, except for the E and F sites, could be associated with a specific minimum (Table 1) located in the immediate vicinity of their van der Waals sphere [26]. No individual minimum was associated with the F sites, but a basin minimum was obtained in the symmetry plane containing the four O_B atoms and bisecting the $O_F \cdots O_F$ line (Fig. 3).

The relative energy values displayed in Table 1 are in perfect agreement with the

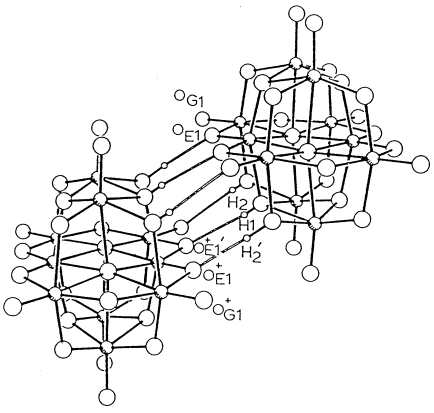

Fig. 2. Perspective ORTEP plot of the $[(H_3V_{10}O_{28})_2]^{6-}$ dimer found in crystalline $H_3V_{10}O_{28}[(C_6H_5)_4P]_3 \cdot 4CH_3CN$. Reproduced from Ref. [23].

Table 1
Computed energy values (hartrees) and relative depth (kcal mol^{-1}) of the 20 minima characterized in the computed MEP distribution of $(V_{10}O_{28})^{6-}$. The values of the critical points [maximum in $-\nabla^2\rho$ (a.u.)] are reported

Site	Computed energy	Relative energy	Multiplicity	$-\nabla^2\rho$
O_B	−0.7201	0.0	4	3.09
O_C	−0.7040	10.1	8	2.83
O_D	−0.6829	23.3	2	2.84
Basin minimum	−0.6818	24.0	2	2.57
O_G	−0.6315	55.6	4	2.61

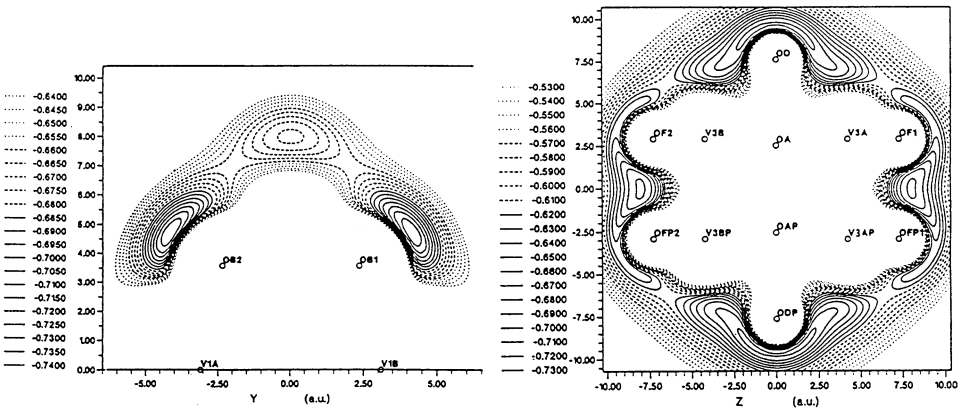

Fig. 3. Planar sections of MEP computed for $[V_{10}O_{28}]^{6-}$. Left: half-plane containing two V and two O_B sites. Right: plane containing the A, D and F sites. Both planes display the basin minimum located in the bisector planes of $O_B\cdots O_B$ and $O_F\cdots O_F$. Contour interval: 0.05 hartrees.

experimental results of Klemperer and coworkers [23,25], since site B is associated with the deepest minimum, followed by site C. The position of the minima associated with sites B and C was determined by computing the MEP distribution on spherical surfaces centred on O_B and O_C, respectively (Fig. 4). Both minima are located away from the symmetry plane containing 12 oxygen and six vanadium atoms, in a direction which exactly fits the direction of the hydrogen bonds characterized in the $[H_3V_{10}O_{28}]^{3-}$ dimer (Fig. 2). Other correlations have been noted with the critical points of charge concentration obtained from the Laplacian distribution of the charge density [27].

How can we explain the energy ordering of the local minima? The electrostatic potential computed in the vicinity of a given atom accounts for both the local and the environmental effects, the respective influence of which cannot easily be separated. A correlation with the critical points of charge concentration which accounts for purely local effects may be of some help (Table 1). The deepest MEP minimum also corresponds to the highest value of $-\nabla^2\rho$, which means that the unique coordination environment of oxygen B might be responsible for its enhanced basic-

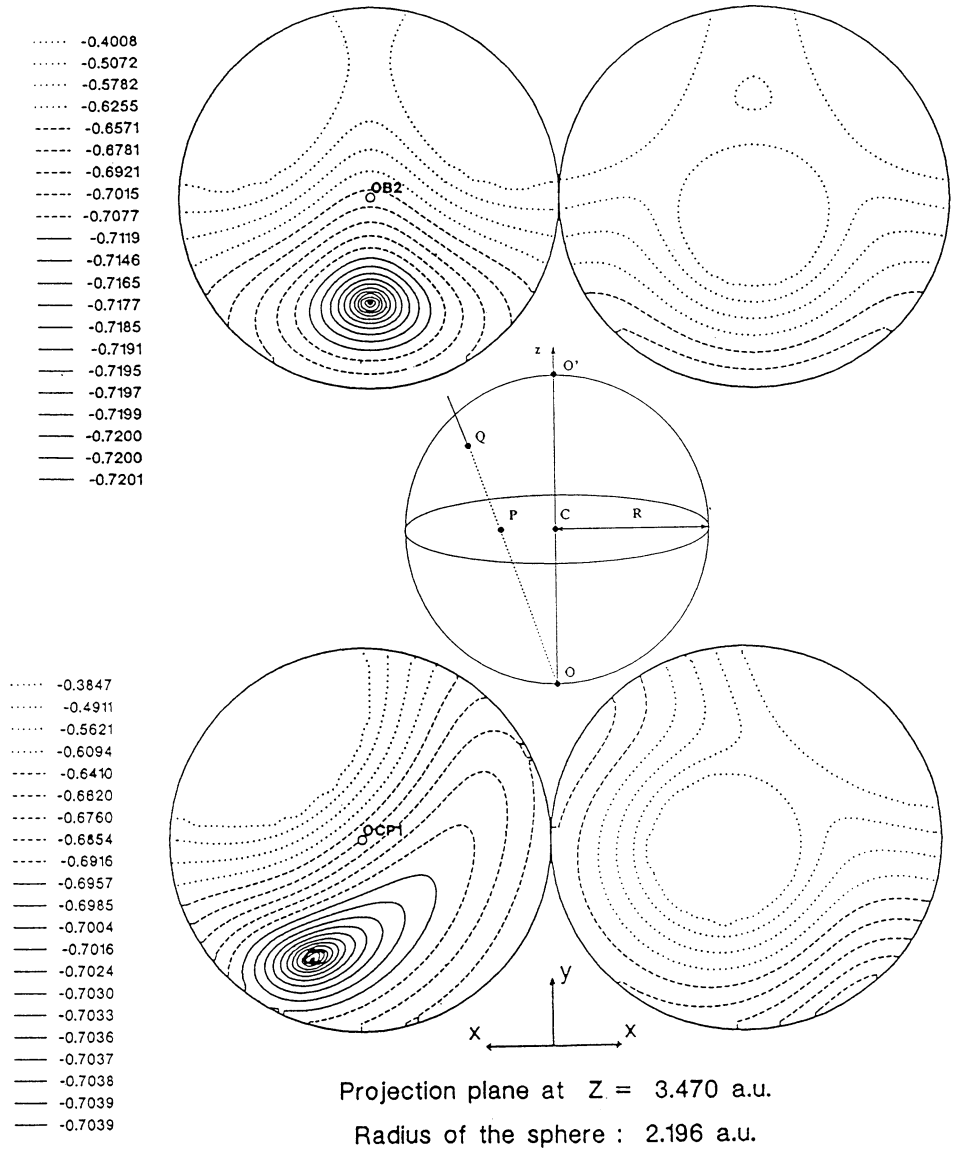

Fig. 4. Principle of the stereographic projection and application to the representation of MEP computed (i) on a sphere centred on O_B (top); (ii) on a sphere centred on O_C (bottom). The projection plane used for both representations contains two O_B and four O_C sites. Lowest contour -0.72009 hartree (top), -0.70395 hartree (bottom); first contour interval 4.8×10^{-5} hartree, successive contour intervals multiplied by 1.5.

ity. O_B is in triply bridging position, coordinated to a tripod of vanadium atoms. Three lone pairs of the formally O^{2-} ligand are taking part in the O–V bonds while the last lone pair is pointing in a direction opposite to the O–V tripod, in fact in the direction of the MEP minimum. This unique lone pair should be assigned the large value of the charge concentration, and consequently, the high basicity of the O_B site along that direction. The correlation between the energy of the MEP minimum and the critical points in $-\nabla^2\rho$ is not so clear-cut for the other sites, indicating that the environment has an influence on the MEP values. As can be expected, the environmental influence is especially important for the basin minimum associated with sites F and B, since this minimum is lower by 30 kcal mol^{-1} than that associated with terminal site G. From purely local criteria, those two sites should be equivalent in view of their critical points of charge concentration. It should be noted that the computed values of the MEP minima are extremely low (-452 kcal mol^{-1} for O_B) due to the high negative charge of the isolated molecule. Those values should not be regarded as approximate protonation energies, since real protonation occurs in an electroneutral medium in which the potential energies are considerably shifted due to the solvent influence. This study just assumes a complete isotropy of the solvent field, reducing its effect to a constant shift without interference with the MEP topology.

3.2. The binary metal complexes $(M_2W_4O_{19})^{4-}$ (M = Nb, V)

Further ab initio SCF studies have been carried out by Maestre et al. on the *cis* conformation of the mixed-metal Lindqvist ions $(M_2W_4O_{19})^{4-}$ (M = Nb, V, Fig. 5)

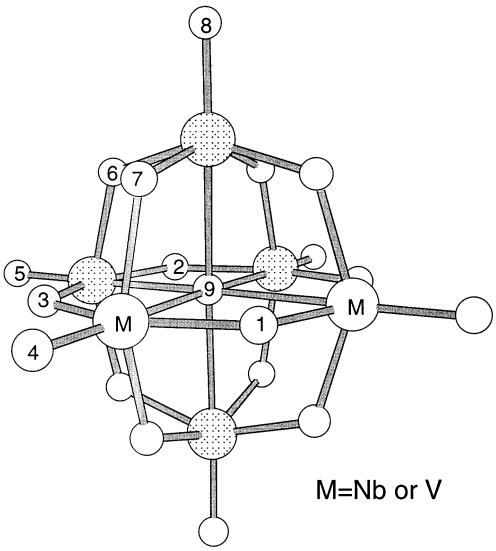

Fig. 5. Structure of $(M_2W_4O_{19})^{4-}$ (M = Nb or V).

investigated experimentally by Klemperer and coworkers [28–32]. Those calculations were aimed at investigating in more detail the influence of the basis set on the MEP topology and at comparing the relative depths of the MEP minima to the relative energies of the corresponding protonated forms [33]. Basis set I (BSI), used for optimizing the geometries of the free ions and of their protonated forms, is of double-ζ quality for all valence electrons. In basis set II, used for single-point calculations on the free ions assuming the geometries optimized with BSI, the valence shell of the oxygen atoms, formally O^{2-}, was described with an extended basis set composed of six s-type and four p-type contracted Gaussians, augmented with two d-type polarization functions. The results are displayed in Table 2.

As for $(V_{10}O_{28})^{6-}$, the bridging oxygens are globally more basic than the terminal ones, but the differences in basicity between the various bridging sites are extremely small. In that context, the quality of the basis set may influence the result as for ions $(V_2W_4O_{19})^{4-}$, where OW_2 was found to have the deepest MEP minimum with the small basis set (Table 2). The use of the large basis set modifies the basicity scale deduced from the sequence of the MEP minima in favour of the oxygen site bridging the two vanadium atoms. The inclusion of diffuse functions in the basis set of oxygen also has an important consequence on the topology of the MEP distribution. With BSI, a single MEP minimum, located in the M–O–M plane, is found in the vicinity of the bridging oxygens. When the large basis set is used, the former minimum becomes a saddle point connecting two distinct minima reminiscent of the oxygen lone pairs:

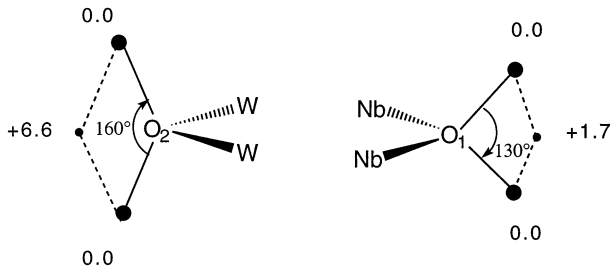

1

Geometry optimization of the various conformers of the protonated complex $(HM_2W_4O_{19})^{3-}$ has been carried out with BSI. The sequence of the computed protonation energies matches that of the MEP minima for both considered molecules, even though the relative energy values may differ by a few kcal mol^{-1} (Table 2).

An interesting result was obtained for $(HV_2W_4O_{19})^{3-}$. The geometry of the protonated complex in its most stable conformation (H attached to OV_2) was found to adopt the C_s symmetry due to a pronounced bending of the hydrogen atom out of the V_2W_2 plane.

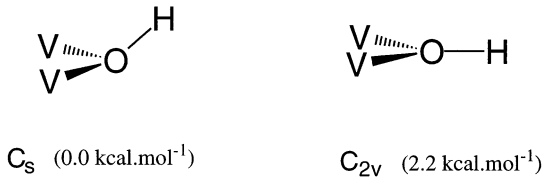

2

Table 2
Relative values of MEP minima (kcal mol^{-1}) computed with basis sets I and II, and relative protonation energies [E_r (kcal mol^{-1})] computed with basis set I for *cis*-$(M_2W_4O_{19})^{4-}$ (M = Nb, V)

Oxygen[a]	Type	M = Nb			M = V		
		MEP		E_r	MEP		E
		I	II	I	I	II	I
1	$O(M_2)$	0.0	0.0	0.0	0.0	0.0	0.0
2	$O(W_2)$	5.3	2.4	3.1	−4.1	2.8	5.2
3	O(NbM)	6.4	3.4	3.8	−0.8	1.4	5.1
4	ONb	16.5	11.6	8.9	36.8	33.4	38.7
5	OW	27.3	24.8	25.4	19.4	27.7	30.1

[a]See Fig. 4 for oxygen numbering.

The MEP distribution computed for this protonated species still displays its lowest minimum on the protonated oxygen OV_2, in the region opposite to the tripod composed of the O–H and of the two O–V bonds. This situation is in fact reminiscent of the triply bridging oxygen site in the decavanadate ion, where an enhanced charge concentration was found in the direction opposite to the three O–V bonds. In the case of the protonated species, however, one can expect that local relaxation and H···H repulsion will prevent the attachment of a second proton to oxygen O_1, in spite of a favourable electrostatic interaction.

4. Interaction between an anionic host and a neutral guest: RCN ⊂ $(V_{12}O_{32})^{4-}$

4.1. MEP distributions

Klemperer and coworkers [13–15] reported the structure of inclusion complexes characterized by the penetration of a nitrile substituent in the hemispheric cavity of a dodecavanadate ion (Fig. 6).

Structural differences have been observed between the inclusion complexes of

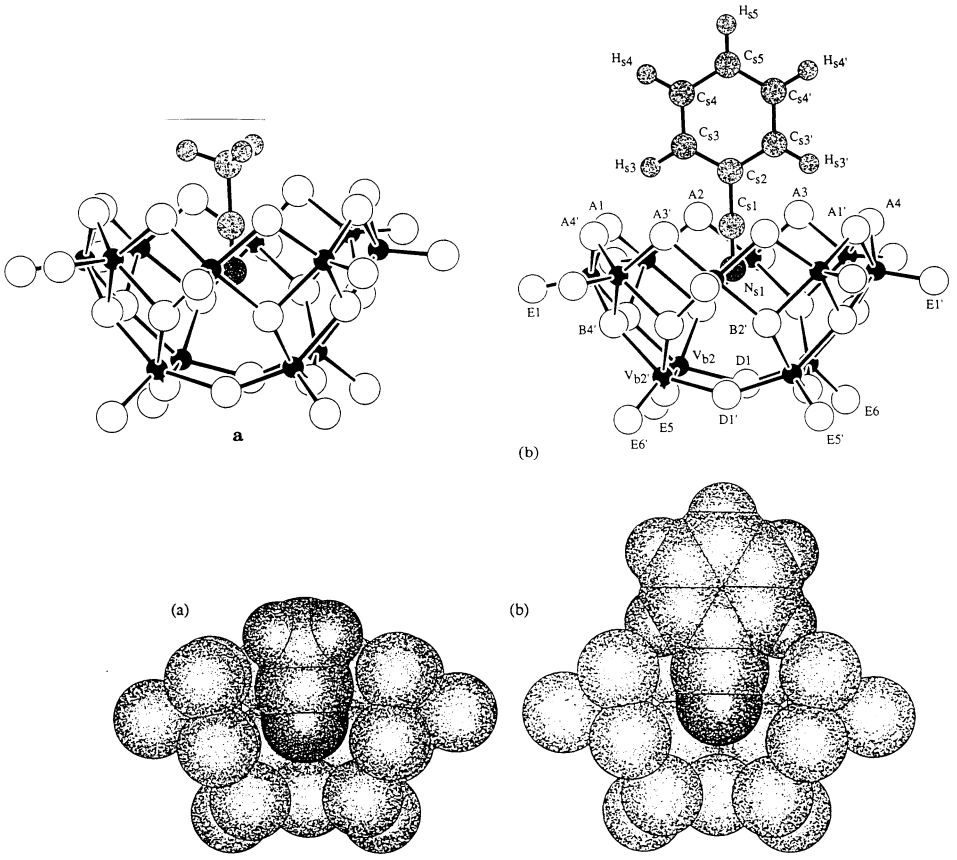

Fig. 6. Perspective and space-filling plots of $RCN \subset (V_{12}O_{32})^{4-}$ (reprinted from Ref. [15] with permission).

acetonitrile and benzonitrile. With benzonitrile, two hydrogen atoms of the phenyl group are in van der Waals contact with four of the eight oxygen atoms forming the rim of the vanadate basket. Acetonitrile does not display such close interactions: even though the nitrile is going slightly deeper into the cavity, the pyramidality of the methyl substituent prevents O···H contacts (Fig. 6). Acetonitrile is therefore "hovering freely" inside and above the cavity, without close interactions either between the nitrile group and the inner side of the cavity or between the methyl substituent and the upper oxygen sites. The observed distance from the nitrile nitrogen to the (V_4) plane at the bottom of the host framework is 2.22 Å, and the average N···V distance reaches 3.28 Å [13–15]. However, the host–guest interaction appears strong enough to persist in solution. Those complexes therefore provide an interesting opportunity to enquire about the nature of the interactions between an anionic host and a neutral, but polar, guest.

Assuming first the interaction to be mainly of electrostatic origin, one could first investigate the MEP distributions of the separate host and guest subsystems and

consider their propensity to associate following the lock and key mechanism defined in Section 2. As evidenced from Fig. 7(a), a dipolar field is created in the accessible part of the host cavity due to the presence of a saddle point in the MEP distribution. This saddle point separates two regions of low potential, one at the top and the other at the bottom of the cavity. The dipolar field generated between the saddle point and the upper MEP minimum is exactly opposite to the permanent dipole of the isolated guests ($\mu = 3.92$ D for acetonitrile, $\mu = 4.18$ D for benzonitrile), as exemplified by the MEP distribution of benzonitrile [Fig. 7(b)].

Superimposing the host and guest MEP distributions at the positions occupied in the inclusion complex makes the potential minimum located in front of the N atom in C_6H_5CN coincide exactly with the MEP saddle point in the host cavity [34].

This electrophilic character of the host cavity was unexpected and appears in complete contrast to the sequence of potential minima which give the external side of the bowl-shaped complex a definite basic character (Fig. 8).

The reasons for such a separation between an electrophilic inside and a nucleophilic outside should be sought in the orientation of the free lone pairs of the doubly and triply bridging oxygens which form the cage. As noted in the previous section, those lone pairs tend to complete a tetrahedron initiated by the metal–oxygen bonds. For either doubly or triply bridging oxygens, the lone pair(s) is (are) therefore oriented external to the local curvature of the cage surface. If the cage considered from the outside is convex [35], then all oxygen lone pairs and the associated charge concentrations will be oriented outside. By contrast, the inner part of the cage, devoid of charge concentration, will become electrophilic. In the opposite way, if the cage presents locally some concave or planar oxygen sites ($\Sigma\theta \approx 360^\circ$), then the charge concentration associated with those sites will be oriented at least in part towards the centre of the cavity. This leads to establishing a correlation between the topology of a metal oxide cage and its acido-basic character which could be termed: *convexity favours basicity*.

Since the work of Klemperer on $RCN \subset (V_{12}O_{32})^{4-}$, other bowl-shaped vanadate clusters have been characterized by Karet et al. [36]. In those smaller $[V_5O_9(O_2CR)_4]^-$ complexes, the doubly bridging oxygen sites which circled the entrance of the cavity have been replaced by less basic carboxylate ligands. The dipolar character of the molecular field is decreased by such a substitution and, quite logically, the new molecule accommodates a single halogen anion, Cl^- or Br^-, in a more uniformly electrophilic cavity.

4.2. The host–guest interaction energy and its decomposition

The interaction energies computed at the SCF level between the $(V_{12}O_{32})^{4-}$ host and the real or model guest molecules HCN, CH_3CN and C_6H_5CN were found to be -12.8 kcal mol^{-1} for HCN (for an optimized position of the guest), -14.4 kcal mol^{-1} for CH_3CN, and -14.1 kcal mol^{-1} for C_6H_5CN (both for the observed position of the guest) [37]. Note that a permanent dipole is required for the guest to be efficiently attracted in the host cavity. Linear, non-polar molecules

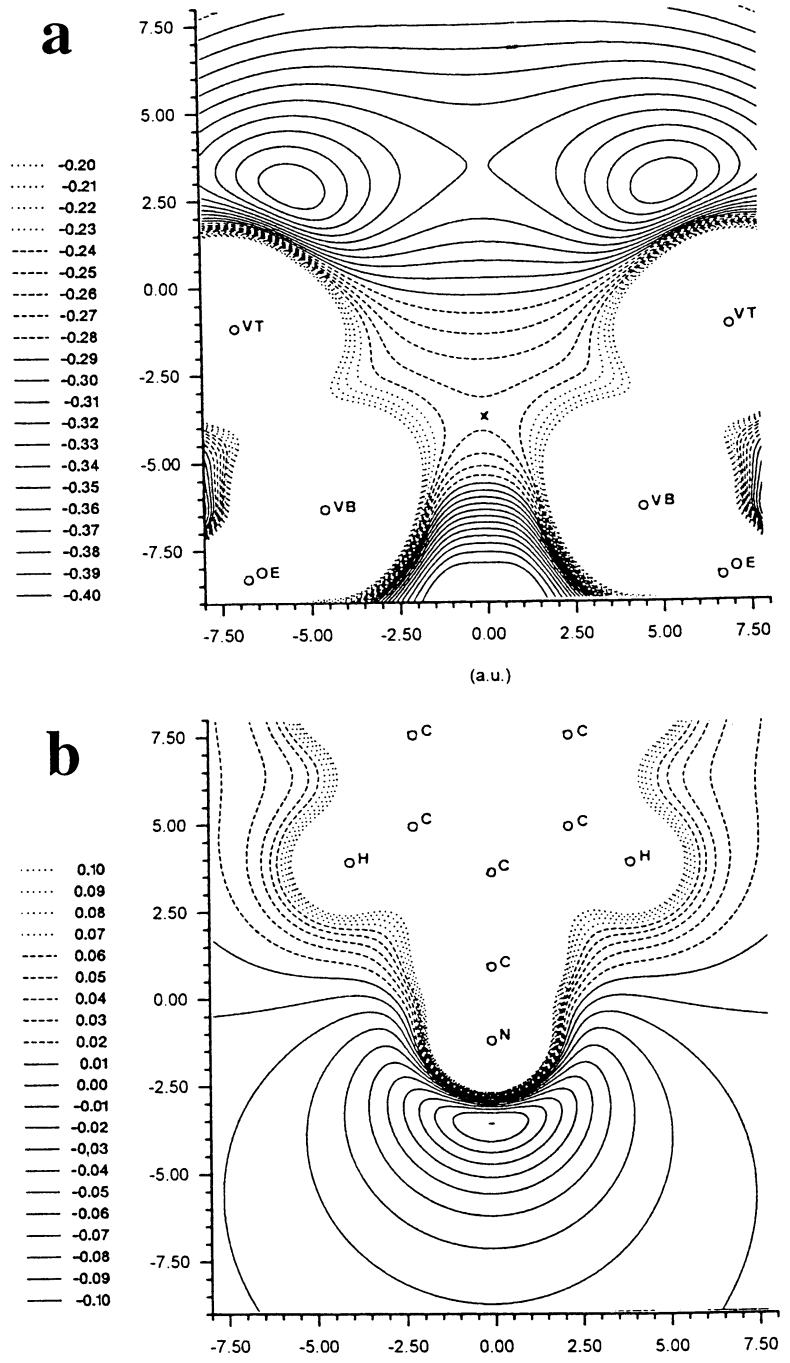

Fig. 7. (a) Molecular electrostatic potential (MEP) distribution computed in the accessible part of the $(V_{12}O_{32})^{4-}$ cavity. (b) MEP distribution computed for C_6H_5CN. (Contour interval: 0.01 hartree).

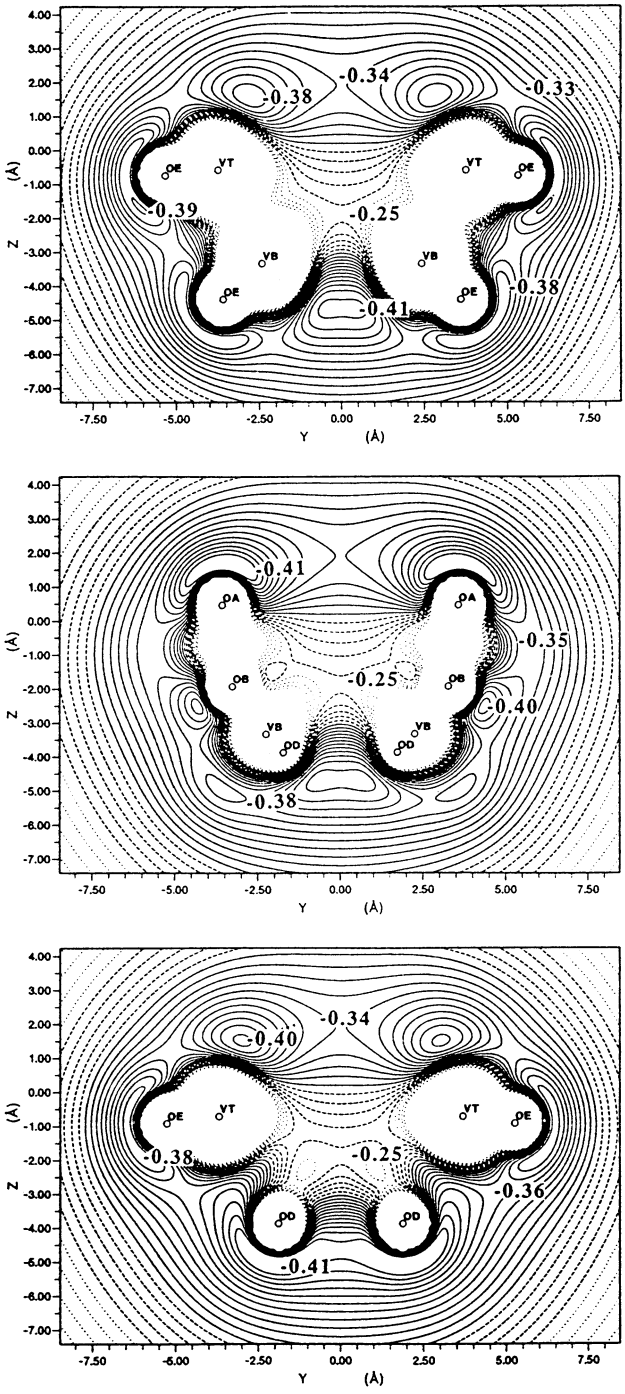

Fig. 8. Maps of the MEP distribution generated by $(V_{12}O_{32})^{4-}$ in three planes respectively containing (a) four terminal (O_E) atoms; (b) two doubly bridging oxygen atoms located at the rim of the cavity [O_A sites, rotated by 21.6° with respect to (a)]; (c) two doubly bridging O_D sites, located at the bottom of the cavity [rotated by 45° with respect to (a)]. Contour interval: 0.01 hartree, distances in Å.

are either weakly attracted (N_2: $E_{inter} = -5$ kcal mol^{-1}) or strongly repelled (C_2H_2: $E_{inter} = +10.6$ kcal mol^{-1}).

The stabilization energies computed for the three R–CN guest molecules correspond to the same order of magnitude, but a deeper insight into the major contributions to those energies shows that the bonding is somewhat different for the HCN model and for the real guest molecules. The decomposition of the interaction energy was carried out by means of the constrained space orbital variation (CSOV) method due to Bagus et al. [38,39]. The procedure uses as starting vectors for the supersystem the wavefunctions obtained at convergence for the separate subsystems, properly orthonormalized. The energy associated with those trial vectors accounts for both the Coulombic interaction and the Pauli repulsion between the subsystems. The energy associated with the polarization of the guest in the field of the host is obtained by achieving the SCF convergence on the guest vectors while freezing those of the host. Then, the set of vectors just obtained for the guest is frozen and the SCF iterations are carried out on the host vectors only, thus yielding the counter polarization of the host due to the guest. Finally, SCF convergence is achieved on the supersystem, which provides the additional stabilization energy due to host–guest orbital interaction, analysed in terms of charge transfers (donation and back-donation). The results of this energy decomposition analysis carried out on $RCN \subset (V_{12}O_{32})^{4-}$ are displayed in Table 3.

When the size of R increases, the growing contacts between R and the host augment the Pauli repulsion which eventually cancels out the Coulombic attraction for $R = C_6H_5$. In the opposite way, the C_6H_5 substituent increases the polarizability of the guest molecule and its contribution to the host–guest attraction. In a similar way, the presence of acceptor orbitals on the R substituent makes possible a charge transfer from the oxygen atoms of the host to those orbitals. The charge transfer energy, computed to be 2.6 kcal mol^{-1} for HCN due to the donation from the C≡N π orbitals, increases to 4.65 kcal mol^{-1} for $R = CH_3$ and to 5.3 kcal mol^{-1} for $R = C_6H_5$ because of the host to guest back-donation. The contribution of charge transfer to the total interaction therefore varies from 20% for HCN to 37% for

Table 3
Decomposition of the stabilization energies [ΔE (kcal mol^{-1})] computed for R–CN molecules in the cavity of the $(V_{12}O_{32})^{4-}$ host

	ΔE				
Guest	Total	Coulomb + Pauli[a]	P^{b}_{guest}	P^{c}_{host}	CT[d]
HCN	−12.8	−5.3	−2.7	−2.2	−2.6
CH_3CN	−14.4	−3.7	−2.5	−3.55	−4.65
C_6H_5CN	−14.1	+1.8	−6.7	−3.9	−5.3

[a]From the energy computed for the supersystem using the orthonormalized wavefunctions of the separated subsystems.
[b]P_{guest} = polarization energy of the guest molecule.
[c]P_{host} = counter polarization energy of $(V_{12}O_{32})^{4-}$
[d]CT = orbital interaction and charge transfer energies.

C_6H_5CN. The higher the contribution of the host–guest orbital interactions, the less the two subsystems should be considered as separate entities linked together by non-covalent interactions. We therefore propose to use the weight of those interactions in the total stabilization energy of the supersystem (not accounting for the monopole–monopole interaction in case of two charged species) to quantify the supramolecular character of the interaction.

4.3. Potential energy of the RCN guest inside and outside the host cage

Taking HCN as a model and assuming the linear guest system to move along the symmetry axis ($\theta = 0$), the host–guest interaction energy (bold line) and its Coulombic part including the Pauli repulsion (dotted line) are represented in Fig. 9.

The Coulombic interaction becomes the dominant and almost exclusive component of the host–guest interaction as soon as HCN is withdrawn from the cage, but this interaction soon becomes repulsive if HCN is not allowed to bend over the symmetry axis. Such a bending has been considered: N is constrained to remain on the axis and θ represents the angle between the axis and the HCN direction. Bending removes the energy barrier and a distinct equilibrium position, not characterized experimentally, is found for $\theta = 180^\circ$ (HCN is again collinear to the symmetry axis, but upside down). Practically all the stabilization energy corresponding to this second minimum is of Coulombic origin, and therefore expected to be extremely sensitive to the influence of the counterions, especially since HCN is not protected any more by the cage. The existence of similar "Coulombic associations" between an isolated $(V_{12}O_{32})^{4-}$ ion and an RCN molecule in upside down position has been verified from calculations carried out with $R = CH_3$ and C_6H_5. It is of interest to note that an acetonitrile molecule has been characterized in the crystal structure of $(NBzEt_3)_2[V_5O_9Cl(O_2CPh)_4]$ [36] with the methyl substituent facing the chlorine ion inserted in the host cavity.

5. Where are the metal electrons in a reduced polyoxoanion?

All species discussed up to now involve fully oxidized, d^0 metal atoms. However, metal oxide clusters can in many instances undergo reduction while maintaining their integrity with only subtle changes in their structure [6,19,40–42]. No theoretical investigation carried out at the ab initio level has been reported yet on such complexes.

An unambiguous determination of the number of reduced metal centres may be a non-trivial problem [19]. One step further, the quantitative analysis of the magnetic data using the Hamiltonian operator $\boldsymbol{H} = \Sigma_{i<j} J_{ij} \boldsymbol{S_i S_j}$ has been carried out for some totally reduced systems such as $K_{12}[V^{IV}_{18}O_{42}(H_2O)]$ or $K_9[H_3V^{IV}_{18}O_{42}(H_2O)]$ [19] and for a series of magnetic nanoclusters involving open-shell metal centres embedded far apart from each other [43]. The problem of the localization/delocalization of the metal electrons in partly reduced species has been addressed mainly by means

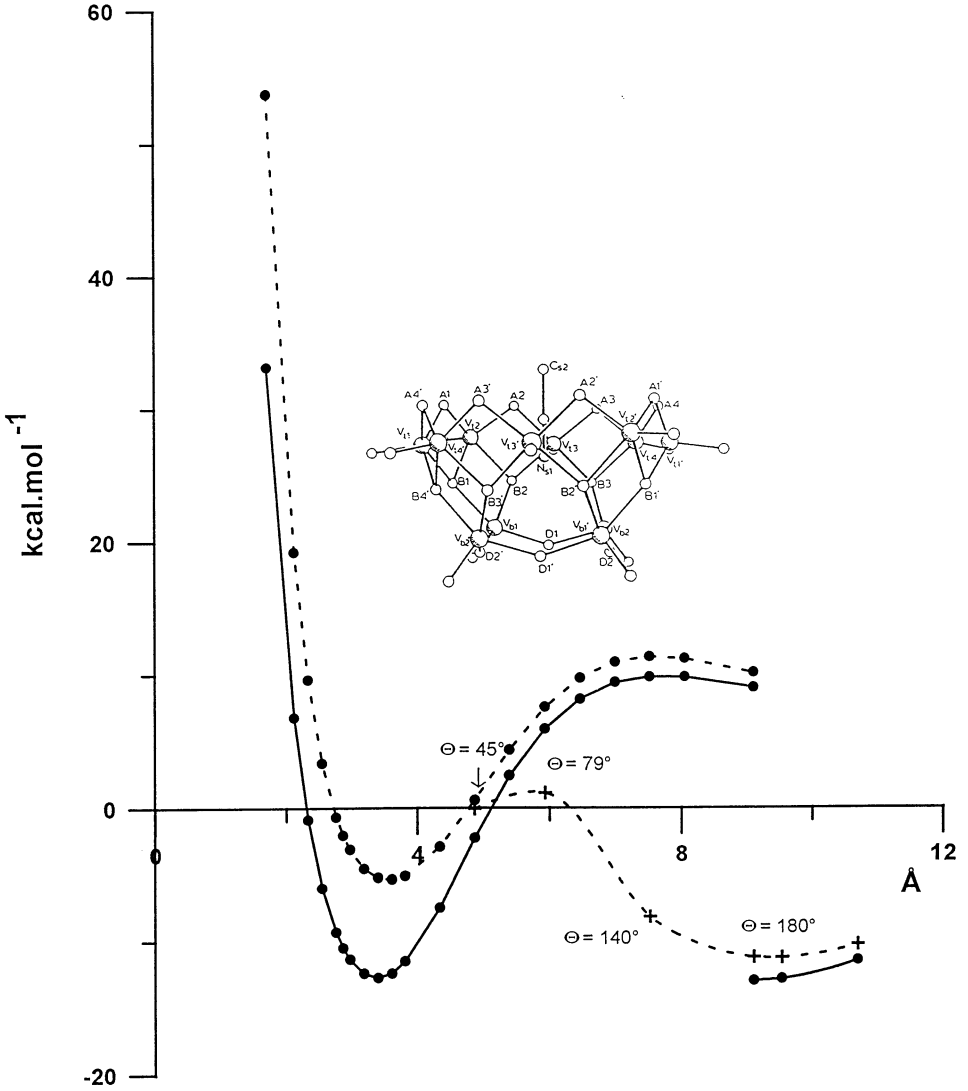

Fig. 9. Total (solid line) and Coulombic (dotted line) host–guest interaction energies (kcal mol^{-1}) computed for HCN⊂$(V_{12}O_{32})^{4-}$ as a function of the position of N on the symmetry axis. The origin of the distances corresponds to the projection of the O_D oxygens on that axis. After the bifurcation point, the dotted line with crosses corresponds to the Coulombic interaction for $\theta \neq 0$ (θ = angle between linear HCN and the symmetry axis). The total interaction energy has been plotted again for $\theta = 180°$ (HCN upside down).

of an interpretation of the EPR spectra [19] and by valence sum calculations based upon the X-ray determined geometries [44].

The synthesis and characterization of the bicapped Keggin complex

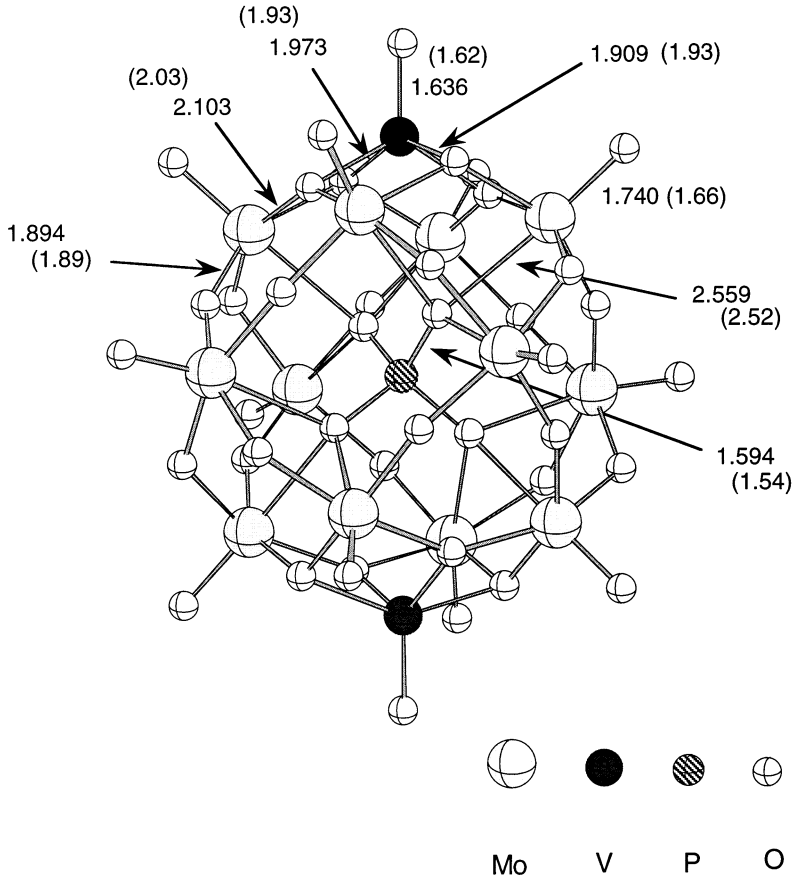

Fig. 10. Optimized bond distances (Å) for the ground state of anion $[PMo_{12}O_{40}(VO)_2]^{5-}$ compared with the experimental values (in parentheses).

$(Et_3NH)_5[PMo_{12}O_{40}(VO)_2]$ reduced by eight electrons has recently been carried out by Chen and Hill [44] (Fig. 10). We report density functional calculations performed on that complex in order to investigate the distribution of the metal electrons over the framework in the real system as well as the relative stabilities of the various reduced species as a function of the number n of metal electrons and accounting for the influence of the crystal field. Calculations were carried out with the ADF program [45] using a triple-ζ + polarization Slater basis set to describe the valence electrons of O. For vanadium, a frozen core composed of the 1s, 2s and 2p orbitals was described by double-ζ Slater functions, 3d and 3s by triple-ζ functions and 4p by a single orbital. An equivalent basis set was used for molybdenum. The valence electrons of P were described by triple-ζ + polarization functions. The geometries and binding energies were calculated using gradient corrections. We used the local spin density approximation characterized by the electron gas exchange ($X\alpha$ with $\alpha =$

2/3) together with Vosko–Wilk–Nusair parametrization [46] for correlation. Becke's non-local corrections [47,48] to the exchange energy and Perdew's non-local corrections [49,50] were added. The calculations on the bicapped cluster were performed under the constraints of the D_{2d} symmetry point group. Some calculations were also carried out with the X-ray geometry using the C_1 symmetry group. Spin-unrestricted calculations were used for the open-shell calculations.

The reference model system used for the calculations was the fully oxidized cluster with net charge +3. The geometry of the $[PMo_{12}O_{40}]^{3-}$ moiety was optimized under the constraints of the T_d symmetry, and then the cluster was completed by adding two VO units with the geometrical parameters taken from the X-ray structure. A complete geometry optimization of the real cluster has also been carried out (Fig. 10).

The relative energies and symmetries of some frontier orbitals of $[PMo_{12}O_{40}(VO)_2]^{3+}$ are reproduced in Fig. 11(a). This diagram shows that the energy gap between the HOMO and the two lowest unoccupied orbitals is very small (0.06 and 0.16 eV). This is a sign of real instability of the fully oxidized complex which will tend to populate the low-lying levels. If we rely on the so-called Aufbau principle, that is, if we assume that the reduction of the complex can be carried out without perturbing the underlying orbitals, then the addition of eight metal electrons should populate orbitals $22b_1$, $22a_2$, $36a_1$, and 57e with two electrons each. Since the latter level is doubly degenerate, a Jahn–Teller distortion could then be expected. One can also note that four metal electrons should be localized on the two V centres, while the four remaining electrons should occupy symmetry orbitals delocalized over the 12 molybdenum atoms.

This oversimplistic description should be corrected, however, due to the relaxation of the inner levels. A calculation on the fully reduced system $[PMo_{12}O_{40}(VO)_2]^{5-}$ shows an energy crossing between the molybdenum levels $36a_1$ and 57e on the one hand, and the vanadium levels $22b_1$ and $22a_2$, on the other hand. This new orbital diagram [Fig. 11(b)] modifies the distribution of the eight electrons. The electronic configuration represented in Fig. 11(b) is a triplet, in which six electrons are delocalized over the 12 Mo centres, whereas two electrons only are accommodated on the vanadium-centred orbitals and each localized on one vanadium atom. The existence of a singlet state with a similar electron distribution and a very small singlet–triplet energy separation is predicted. The triplet state corresponding to an equi-repartition of the eight electrons between the Mo and the V sites is less stable by 1.41 eV than the electronic structure of minimal energy. The distribution of the electrons in the configuration of lowest energy is in complete agreement with the prediction of Chen and Hill [44], who proposed from valence sum calculations [51] that the V centres are in the +4 oxidation state while the Mo centres are in the +5/+6 oxidation states.

An important question raised by those partly reduced complexes is how many electrons are susceptible to be accommodated on the metal framework. When the system is considered isolated, a region of minimal energy is obtained for anions with net charges −2 and −3, corresponding to five to six metal electrons (Fig. 12). This curve confirms the propensity of the molybdenovanadophosphate cage to accept electrons. However, the calculation carried out on the isolated system can hardly

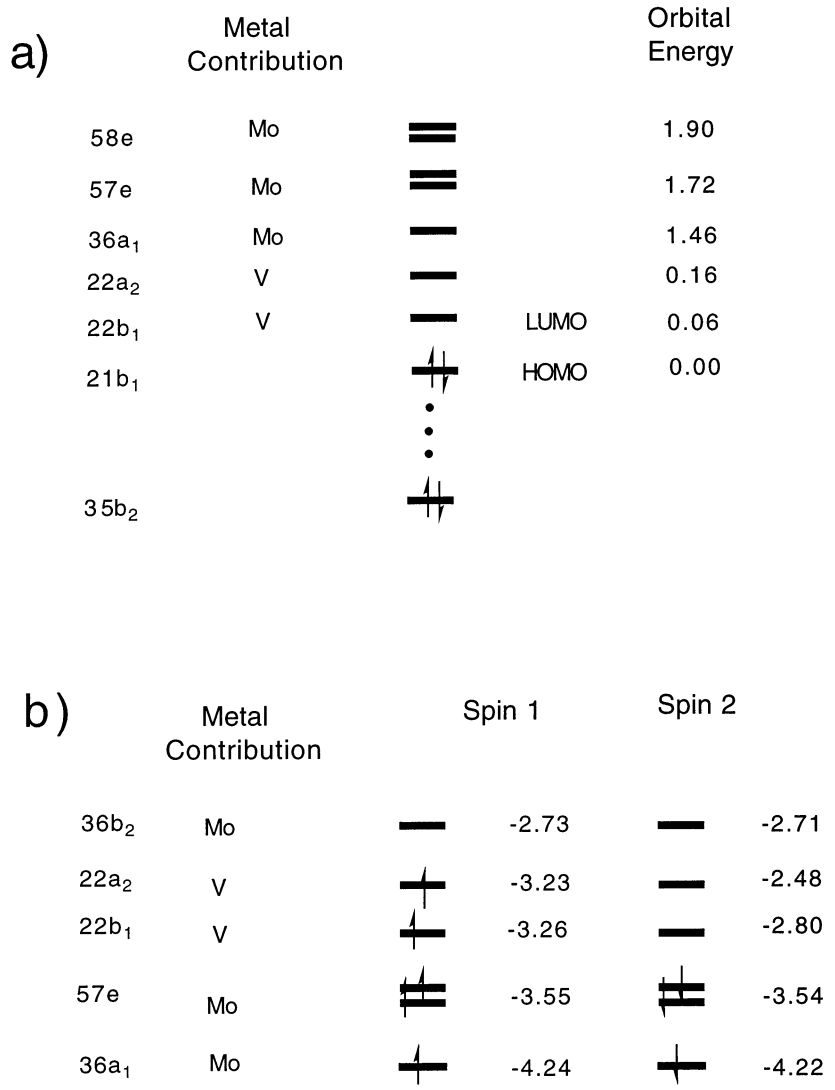

Fig. 11. (a) Symmetry, occupations and relative orbital energies (eV) for the fully oxidized cluster $[PMo_{12}O_{40}(VO)_2]^{3+}$. (b) Symmetry, occupations and energies (eV) of the metal orbitals for the triplet state of lowest energy of anion $[PMo_{12}O_{40}(VO)_2]^{5-}$ in the presence of a charged sphere of diameter equal to 20 Å which generates at the centre of the molecule a potential of +0.393 a.u., the estimated potential due to the crystal.

reproduce the optimal number of electrons to be accommodated in the real molecular environment. The presence of counterions in the vicinity of the cage anion will raise the potential and increase the tendency of the cluster to accept electrons until an equilibrium is obtained, giving rise to the observed crystal.

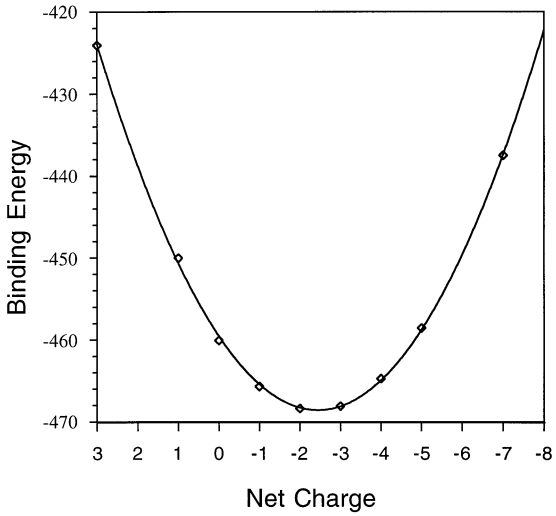

Fig. 12. Binding energies (eV) vs. the net charge of the anion for the isolated cluster (see text).

Two procedures have been used in order to model the crystal field. One of those procedures, detailed in Section 6.2, reproduces the electrostatic potential generated by the crystal by means of an isotropic field created by a charged sphere located at a large distance from the cluster (model I). In another procedure (model II), the cluster is surrounded by 14 point charges located at the centre of mass of the 14 Et_3NH molecules which form the first shell of counterions. In model II, the electroneutrality of the global system has been maintained by attributing each point charge a fractional value of $+5/14$e. The calculations carried out with both models do not change the nature of the ground state for $[PMo_{12}O_{40}(VO)_2]^{5-}$, but dramatically decrease the energies of the frontier orbitals without altering the HOMO–LUMO gap.

Both models confirm that the presence of the crystal field indeed increases the propensity of the cluster to accept electrons. With model II, the energy minimum with respect to the number n of metal electrons is reached exactly for the value of n corresponding to the observed reduced species ($n=8$). With model I, the equilibrium is shifted further, since the cluster energy is lower by 1.48 eV when assuming $n=9$.

6. Stabilization of electronically inverse systems

6.1. Template formation in solution

Polyoxometallate hollow cages are never empty. This requirement for having a water molecule [16–19], a single atomic ion [19,21,52–54], a molecular anion ([12] and references cited therein), cation/anion aggregates [55], or even a metal oxide cluster [9,12,56,57], embedded into a host cavity which seems to be shaped by the enclosed molecule, has strongly suggested, if not yet proved, the template mechanism

of cluster condensation. This template-controlled formation of electronically inverse hosts, however, presents the puzzling case of an attractive interaction between negatively charged species first in solution, during the dynamic process of cluster assembly, and then in the crystal. Mechanisms have been proposed which rely on the presence in solution of ionized fragments of the V_2O_5 lattice and on the well-documented propensity of the (VO_5) pyramid to be assembled in a wide variety of forms [20]. The presence of cations in the solution helps orient the vanadyl $V^{\delta+}=O^{\delta-}$ dipoles opposite to the template ions X^-. However, a crucial point which remains unexplained up to now is the origin of the interaction which forces the oriented vanadate fragments to bend flexibly over the template anion and eventually to get assembled, thus encapsulating X^-. The MEP calculations on $(V_{12}O_{32})^{4-}$ reported in the previous section suggest a driving force to the encapsulating process. The X^- ion moving in solution tends to minimize its electrostatic energy by shifting towards a region with a relatively high electrophilicity or by influencing its environment in order to create such a region. According to the proposed correlation between the topology of a polyoxometallate cluster and its acido-basic properties, the environment most favourable to an X^- ion among vanadate fragments will correspond to the formation of a fully concave metal oxide surface.

6.2. *Guest anions stabilized by the crystal field*

We have applied quantum chemical modelling to two typical examples of electronically inverse hosts, $[H_4V_{18}O_{42}]^{8-}$ (**1**) and $[V_7O_{12}(O_3PR)_6]^-$ (**2**) [21] (Fig. 13), characterized each with an encapsulated halogen guest, but strongly differing in the negative charge of the host cage.

Calculation of the MEP distribution associated with the non-protonated model cage $[V_{18}O_{42}]^{12-}$ and with the tetra-protonated host confirms the presence of a shell of low potentials on the outer surface of the cage, with two types of minima:

(i) potential minima surrounding the terminal oxygens;

(ii) regions of low potential associated with the lone pair of triply bridging oxygens and opposite to the tripods of O–V bonds. Those low potentials extend towards the centre of metal–oxide rings each composed of three oxygen and three vanadium atoms, and coalesce into "basin minima" (Fig. 14).

For both the protonated and the non-protonated hosts, the potential value in those deepest MEP minima is lower by 0.16 to 0.18 a.u. ($\sim$4 eV) than the MEP value obtained at the centre of the cage. The protective influence of the concave host is not sufficient, however, to fully counteract the basicity generated by the high negative charge. The MEP value at the centre is ~ -1 a.u. for the non-protonated model and -0.57 a.u. for $[H_4V_{18}O_{42}]^{8-}$. This latter value still corresponds to an electrostatic energy of $+358$ kcal mol^{-1} for an encapsulated negative charge, which would clearly make the encapsulation process impossible.

When the negative charge of the host is decreased to one electron as in the vanadophosphate cage **2**, then the shielding effect exerted by the concave cage modifies the sign of the potential, which becomes attractive towards a negative

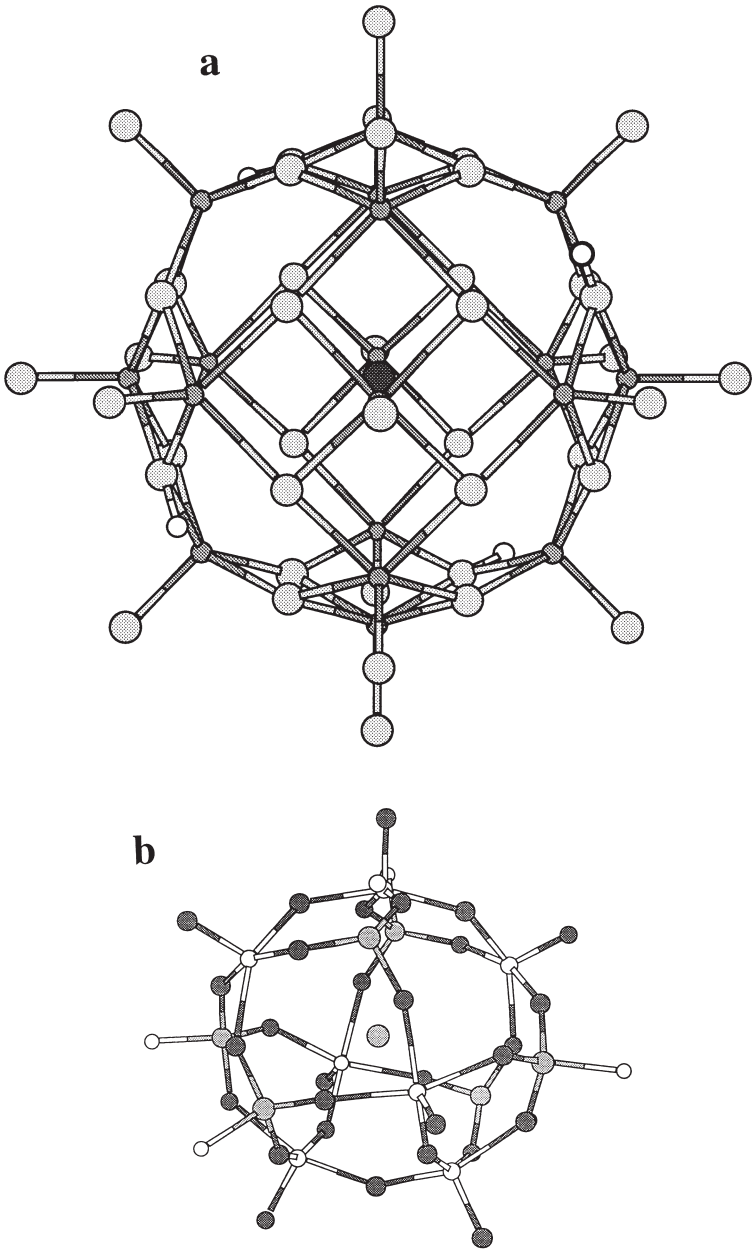

Fig. 13. (a) XMol (Minnesota Supercomputer Center, Inc., 1995) perspective views of the $(X@H_4V_{18}O_{42})^{9-}$ complex assuming a perfect O_h symmetry for the $V_{18}O_{42}$ host cage. The positions of the four protons have been optimized. (b) XMol representation of the $[Cl@V_7O_{12}(O_3PR)_6]^{2-}$ complex from the crystal parameters.

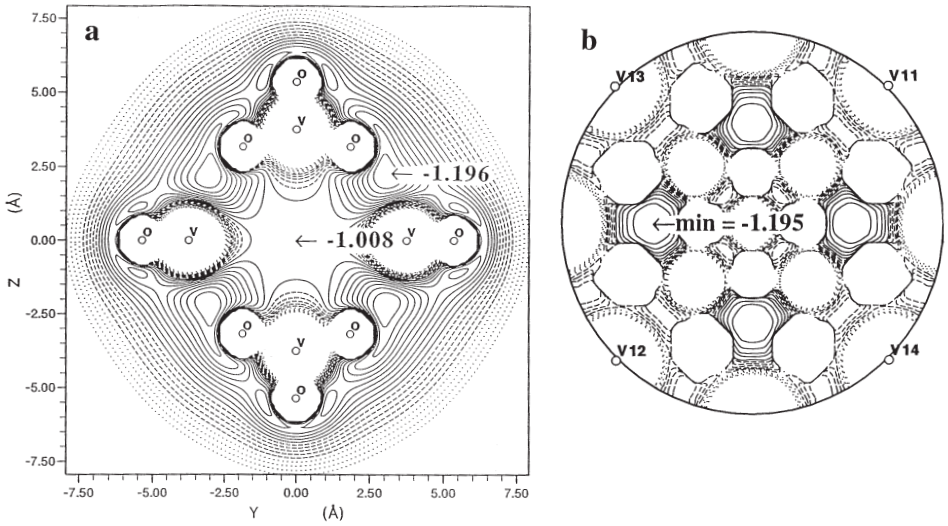

Fig. 14. (a) Maps of the MEP distributions computed for the isolated cage model $(V_{18}O_{42})^{12-}$ (O_h symmetry assumed) in the plane containing the centres of four metal oxide rings and the corresponding "basin minima" of the MEP distribution. (b) Stereographic projection of the MEP distribution computed on a half-sphere concentric to $(V_{18}O_{42})^{12-}$ and with radius $r = 3.7$ Å. The same basin minima appear on the projection plane.

charge. The potential value calculated in the cavity of $[V_7O_{12}(O_3PR)_6]^-$ is $+0.06$ a.u. ($+1.4$ eV), showing that a negatively charged host, even isolated, can be attractive towards a negatively charged guest.

The results obtained with $[H_4V_{18}O_{42}]^{8-}$, however, clearly show that the external field has to be included in some way to achieve the stability of the system. This has been carried out by means of the following procedure.

(i) Model the surrounding crystal by a set of point charges.

(ii) Determine the electrostatic potential generated at the centre of the studied molecule by the point charges contained in successive shells of unit cells, until convergence is reached. The total charge and the dipole moment of the generated crystal fragment should be zero. Then, the lattice potential is given by:

$$\sum_i^{\text{lattice}} \frac{q_i}{r_i} - \sum_j^{\text{unit cell}} \frac{2\pi}{3V} q_j r_j^2$$

where the second term corrects the surface effects generated by a non-zero quadrupole moment in the unit cell. V is the volume of the unit cell and r_i is the distance of the point charge q_i to the origin. Those calculations have been carried out by means of the ELECTROS program [58].

(iii) Define a charged sphere centred on the studied molecule and of diameter equal to 20 Å. The charge of the sphere is defined so as to reproduce the value of the potential at the centre obtained in the previous step. The definition of the

charged sphere approximates the effect of the crystal environment by a field which is constant and isotropic in the molecular domain.
(iv) Carry out a new SCF calculation with a flexible basis set in the presence of the charged sphere.

The value of the lattice potential may be sensitive to the set of point charges assigned to the various atoms of the crystal, especially because of the quadrupole moment correction. For $Cs_9(X@H_4V_{18}O_{42})$, five sets of point charges have been considered which are displayed in Table 4, with the corresponding values of the generated lattice potential. In set 1, the whole anion $(X@H_4V_{18}O_{42})^{9-}$ has been represented by a point charge of -9 assigned to atom X. This representation, which is equivalent to considering the vanadate cage as a uniformly charged sphere, generates the highest lattice potential, $+0.839$ a.u. Then, the computed lattice potential decreases as the charge difference between vanadium and oxygen increases. The largest anisotropy in the charge distribution of the host cage was obtained by assigning to V(IV) and oxygen atoms their formal charges of $+4$ and -2, respectively (set 5 in Table 4; the charge assigned to bridging oxygens was uniformly decreased to -1.833 to account for the presence of the four protons). With that set of charges, the lattice potential was reduced by half, to $+0.426$ a.u. The value corresponding to the intermediate Mulliken charge distribution (charge set 3, Table 4) is $+0.628$ a.u. For all considered sets of charges except the last one, largely unrealistic, the resulting potential at the centre of the empty host becomes positive, that is, attractive towards an anion. The potential distribution computed assuming

Table 4
$Cs_9(X@H_4V_{18}O_{42})$ values of the lattice potential (atomic units) computed by assigning the crystal atoms with various sets of point charges. The contribution to the potential of the point charges generated by successive shells of unit cells is summed up until convergence is reached. The total charge and the dipole moment of the generated crystal fragment are zero. The final value is obtained by adding the correction Q_{corr} induced by the existence of a non-zero quadrupole moment

	Set 1	Set 2	Set 3[a]	Set 4	Set 5
Point charges (e)					
Cs	+1.0	+1.0	+1.0	+1.0	+1.0
X	−9.0	−1.0	−1.0	−1.0	−1.0
V	0.0	+1.0	+1.54	+2.0	+4.0
O (terminal)	0.0	−0.5	−0.78	−1.047	−2.0
O (bridging)	0.0	−0.708	−0.903	−1.047	−1.833
$Cs_9(X@H_4V_{18}O_{42})$ (total)	0.0	0.0	0.0	0.0	0.0
Components of the lattice potential at the origin (a.u.)					
$\Sigma q_i/r_i$	+0.652	+0.687	+0.690	+0.698	+0.716
Q_{corr}	+0.187	−0.005	−0.058	−0.111	−0.290
Total	+0.839	+0.682	+0.632	+0.587	+0.426

[a] Charges deduced from the Mulliken analysis. The charge of the four protons has been averaged on the 24 bridging oxygen atoms.

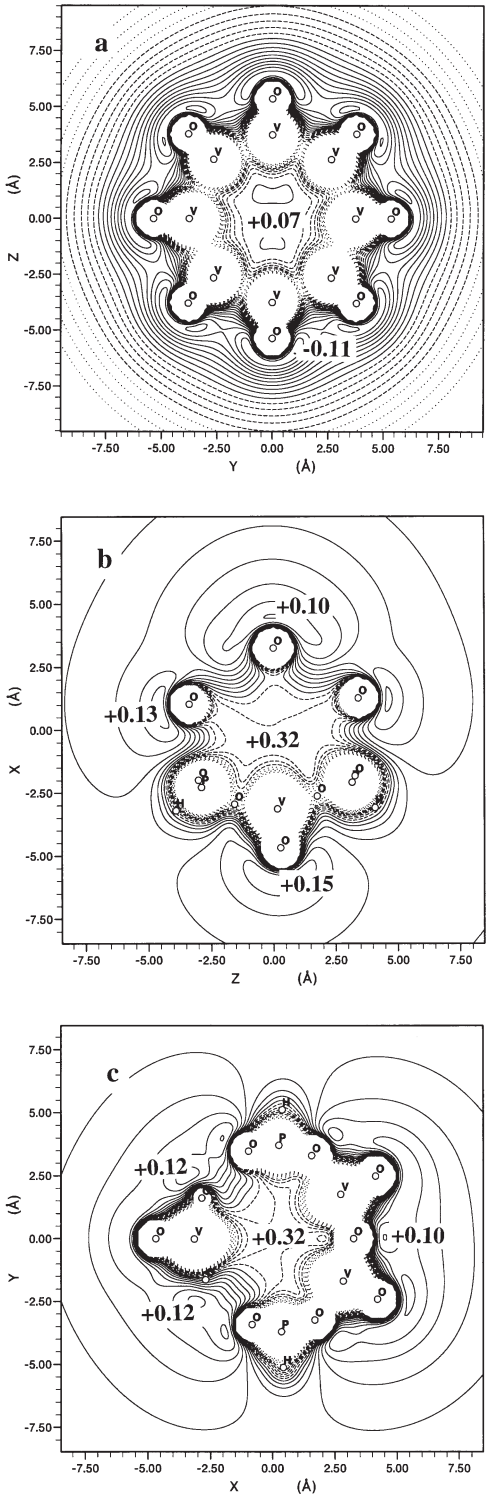
a
+0.07
-0.11
Z (Å)
Y (Å)
b
+0.10
+0.13
+0.32
+0.15
X (Å)
Z (Å)
c
+0.12
+0.32
+0.10
+0.12
Y (Å)
X (Å)

the Mulliken set of charges is displayed in Fig. 15(a) and corresponds to a value of +0.07 a.u. at the centre of the cage.

The Schlemper complex $K_{12}(H_2O@V_{18}O_{42})$ [16] is made of the same host cage, but accommodates a charge of −12 and does not encapsulate an anion, but a water molecule. Its structure has recently been characterized by Müller et al. [19]. A set of point charges transposed from the Mulliken set used for $Cs_9(X@H_4V_{18}O_{42})$ (+1.54 for V, −0.78 for terminal oxygens, −1.07 for bridging oxygens, 0 for H_2O) produces at the centre of the host cage a lattice potential of +0.929 a.u. The simple superposition of this crystal potential on the value of −1.008 a.u. computed for the isolated $(V_{18}O_{42})^{12-}$ cage now yields a negative value of −0.08 a.u. at the centre of the cage. This result does not really prove that the Schlemper complex could not self-organize around a negatively charged atom since, in such a case, the total charge of the complex ion would be −13 and a different crystal organization would be observed. However, it seems that the potential distribution does not favour in such a case the formation of the complex from an anionic template.

The calculation of the potential distribution in the free $[V_7O_{12}(O_3PH)_6]^-$ host cage already yields a positive value at the centre (+0.06 a.u.). Modelling the $[P(C_6H_5)_4]^+$ counterions by positive charges of +1 located on the P atom yields a lattice potential of +0.256 a.u. A more sophisticated charge distribution (+0.472 on phosphorus, −0.068, +0.022, +0.022, +0.048, +0.048, +0.060 on phenyl carbons) practically does not modify the potential at the centre (+0.251 a.u.). The electrostatic energy undergone by the guest chlorine ion amounts in this case to +0.32 a.u. [Fig. 15(b, c)]. This value has to be compared with the potential generated on a Cl site by a CsCl cubic crystal environment calculated with the same point charge model (+0.26 a.u.).

The results eventually obtained for the considered host cages confirm that topological factors are sufficient to raise the potential values in the cavity by 0.1 to 0.2 a.u. with respect to the external side. The simple shape of the host therefore has an influence which might be decisive in the thermodynamic balance of the complex formation.

It has been evidenced from structural data, infrared spectra, and also from the pre-edge peak of X-ray absorption spectra that strong covalent or ionic interactions between the guest anion and the positively charged vanadium centers should be ruled out when the charge of the guest is not too high [8,9,12,19,55]. There are exceptions such as $Na_6[(F\cdots F)@H_6V_{12}O_{30}]\cdot 22H_2O$ for which strong V–F contacts (2.17 Å) have been observed [8]. However, most guest ions with a single negative charge give the impression of hovering freely in the accessible region of the host cavity. This lack of directional, orbital-driven interaction between the guest ion and

Fig. 15. Maps of the electrostatic potential computed for the host cages $(H_4V_{18}O_{42})^{8-}$ (a) and $[V_7O_{12}(O_3PR)_6]^-$ (b, c) in the presence of a charged sphere of diameter 20 Å reproducing the potential generated by the crystal at the centre of the host cage [+0.632 a.u. for $Cs_9(H_4V_{18}O_{42}Cl)$ assuming a set of point charges deduced from the Mulliken population analysis, see Table 4; +0.256 a.u. for $(Ph_4P)_2(V_7O_{12}(O_3PPh)_6Cl)$]. (a) $(H_4V_{18}O_{42})^{8-}$, plane containing eight terminal oxygens. (b, c) Two sections of the MEP distribution of $[V_7O_{12}(O_3PH)_6]^-$. Contour interval: 0.02 a.u.

specific metal atoms of the host cage does not preclude the existence of a potential energy for the encapsulated anion. This potential energy, important in some cases, should be traced to the electrostatic field generated by the host cage and by the surrounding crystal. The field generated by the host cage alone is quite isotropic inside the cavity and generates a potential which is generally repulsive toward a guest anion, especially when the charge of the host is high. As first suggested by Müller [12], accounting for the crystal environment generates a favorable environment for the encapsulated guest anion (except in the case of the Schlemper complex), and the magnitude of the resulting potential may in some cases compare to that of ionic crystals. The lack of a significant field gradient inside the cavity and the absence of specific, directional interactions with the metal atoms may explain why the guest molecules give the impression of being loosely attached in the cavity, even though they may benefit from a large potential energy of electrostatic origin.

6.3. Topological criteria for shaping the host cage

It has often been noted that the assembly of the flexible and versatile metal oxide fragments closely followed — and was probably determined by — the shape and symmetry of the small guest molecule [8,9,12,57]. This adaptation is easily exemplified by some typical complexes: atomic guest anions such as X^- (X=Cl, Br, I) are encapsulated in spherical cages, whereas the linear N_3^- ion generates ellipsoidal cages composed of two fused half-shells arranged in D_{2h} symmetry [9,59]. Replacing N_3^- by the tetrahedral ClO_4^- ion generates a cage made of similar fragments rotated by 90° in order to reflect the tetrahedral symmetry of the guest ion [9]. The planar assembly of two NH_4^+ and two Cl^- ions is surrounded by a flattened cage with formula $V_{14}O_{22}(OH)_4(H_2O)_2(PhPO_3)_8$ [43].

As long as covalent, or charge transfer, contributions do not become dominant in the host–guest interaction, another, more subtle, correlation could be emphasized between the topology of the host cage and the MEP distribution of the guest. The most typical example of that correlation is given by comparing the cages which encapsulate anionic and cationic guests. As already noted, the metal oxide cages enfolding atomic anions are convex — or concave if considered from the inside — and generate an isotropic potential allowing the guest atom to hover within the cage. In the "electronically normal" complexes exemplified by Khan's $[Na@Mo_{16}O_{40}(OH)_{12}]^{7-}$ system [10,11], the Na^+ ion is encapsulated in an irregular cage in which four triply bridging oxygen atoms break the concavity. Those four atoms have three lone pairs oriented inside the cage, thus inducing a nucleophilic field with tetrahedral symmetry directed towards the sodium atom. A similar host–guest complex in which the sodium guest cation is replaced by two protons was recently characterized by Müller et al. [60].

Local deviations from concavity/convexity are also observed in the host cages encircling strongly polar polyatomic guests. An extreme case is provided by the $(2NH_4^+, 2Cl^-)$ guest system [55]. The host cage associated with that fragment of the NH_4Cl ionic lattice is composed of two $V_5O_9(PhPO_3)_4$ perfectly convex, hemispherical subhosts each facing a chlorine atom and connected to each other by

divanadate bridges. The eight oxygen atoms linking the vanadate bridges to the vanadophosphonate subhosts clearly break the convexity of the cage and provide lone pairs directed towards the ammonium cations. The $(H_2V_{18}O_{44})^{4-}$ host associated with the azide ion [9] tends, although less conspicuously, towards a similar distortion. The four doubly bridging oxygens which face the central nitrogen atom of the azide ion define a local curvature close to zero (the sum of the angles around those atoms is equal to 357°) on the metal oxide polyhedron. This existence of such a "flat" region on the host cage can be related to the charge distribution in the N_3^- ion which can be represented in a rather simplistic way by the alternation scheme $N^-N^+N^-$. In that sense, the azide ion behaves as a cation/anion system and the host topology tends to adapt to the local changes in the MEP distribution of the guest molecule by increasing the basicity in the central region of the cage. Note that this adaptation process is distinct from a plain adjustment to the shape of the guest ion. The necessity for the host to adopt an ellipsoidal shape did not require the local planarity of the cage, which is clearly designed to keep the doubly bridged oxygens relatively close to the central nitrogen (3.2 Å) and to generate in the vicinity of this positively charged atom a toroidal region of low potentials.

7. Conclusion

The ab initio determination of the electrostatic potential distributions induced by polyoxometalate clusters provides guidelines allowing us to explain and predict the behaviour of those species in case of an attack from protons or cationic groups. The trend towards a partial or complete reduction of the metal framework in some of those complexes has been evidenced from DFT calculations. This trend already exists in the isolated cluster, and is enhanced by the upward shift of the electrostatic potential generated by the surrounding cations. An equilibrium is eventually reached, resulting in the observed crystal. The calculations stress the influence of the crystal field which shifts the number of electrons which can be accommodated in the metal framework of complex $[PMo_{12}O_{40}(VO)_2]^{5-}$ from five to six in the free cluster to eight in the observed crystal and possibly more in a different crystal environment.

The electrostatic potential distribution generated by polyoxometalate host cages sheds some light on the stabilization of inclusion and encapsulation complexes. The electrostatic stabilization of such complexes is operative through a lock and key mechanism between the MEP distributions of the host and of the guest subsystems. For $RCN\subset(V_{12}O_{32})^{4-}$ the permanent dipole of the guest molecule favourably interacts with a dipolar field generated inside the host cavity and oriented in the opposite direction. A calculation of the host–guest interaction energy and its decomposition into electrostatic, polarization and charge transfer terms shows that orbital interactions account for 20–37% of the stabilization.

The encapsulation of negatively charged species into negatively charged hosts is favoured by the convex shape of the host which allows the oxygen atom lone pairs to point towards the external side of the cage. This correlation between the topology and the acido-basic character of the host helps our understanding of the template

formation of the host: the vanadium oxide fragments in solution tend to adopt a concave shape in the vicinity of the guest anion in order to maximize the electrostatic potential. The topology of highly charged hosts is not sufficient, however, to stabilize the guest anion. The presence of countercations generates an upfield shift which appears sufficient in most cases to ensure the thermodynamic stability of the host–guest complex. Finally, an examination of some encapsulation clusters involving more complex guests such as N_3^- or $(NH_4Cl)_2$ shows that the host cage tends to adapt not only to the shape of the guest system, but also to its MEP distribution.

Acknowledgements

Calculations were carried out partly on the Cray C98 and on the Cray T3D computers of the Institut du Développement et des Ressources en Informatique Scientifique (IDRIS, Orsay, France), and partly on workstations purchased with funds provided by the DGICYT of the Government of Spain and by the CIRIT of the Generalitat de Catalunya (Grants No. PB95-0639-C02-02 and SGR95-426). We are pleased to thank Professor Nour-Eddine Ghermani for stimulating discussions.

References

[1] A. Müller, Nature 352 (1991) 115.
[2] V.W. Day, W.G. Klemperer, O.M. Yaghi, Nature 352 (1991) 115.
[3] P.C.H. Mitchell, Nature 352 (1991) 116.
[4] M.T. Pope, Nature 355 (1992) 27.
[5] L. Suber, M. Bonamico, V. Fares, Inorg. Chem. 36 (1997) 2030.
[6] A. Müller, J. Döring, Z. Anorg. Allg. Chem. 595 (1991) 251.
[7] A. Müller, E. Krickemeyer, S. Dillinger, H. Bögge, A. Stammler, J. Chem. Soc., Chem. Commun. (1994) 2539.
[8] A. Müller, R. Rohlfing, E. Krickemeyer, H. Bögge, Angew. Chem. Int. Ed. Engl. 32 (1993) 909.
[9] A. Müller, E. Krickemeyer, M. Penk, R. Rohlfing, A. Armatage, H. Bögge, Angew. Chem. Int. Ed. Engl. 30 (1991) 1674.
[10] M.I. Khan, A. Müller, S. Dillinger, H. Bögge, Q. Chen, J. Zubieta, Angew. Chem. Int. Ed. Engl. 32 (1993) 1780.
[11] M.I. Khan, Q. Chen, J. Salta, C.J. O'Connor, J. Zubieta, Inorg. Chem. 35 (1996) 1880 and references cited therein
[12] A. Müller, H. Reuter, S. Dillinger, Angew. Chem. Int. Ed. Engl. 34 (1995) 2328.
[13] V.W. Day, W.G. Klemperer, O.M. Yaghi, J. Am. Chem. Soc. 111 (1989) 5959.
[14] W.G. Klemperer, T.A. Marquart, O.M. Yaghi, Angew. Chem. Int. Ed. Engl. 31 (1992) 49.
[15] W.G. Klemperer, T.A. Marquart, O.M. Yaghi, Mater. Chem. Phys. 29 (1991) 97.
[16] G.K. Johnson, E.O. Schlemper, J. Am. Chem. Soc. 100 (1978) 3645.
[17] G. Huan, M.A. Greaney, A.J. Jacobson, J. Chem. Soc., Chem. Commun. (1991) 26.
[18] A. Müller, J. Döring, Angew. Chem. Int. Ed. Engl. 27 (1988) 1721.
[19] A. Müller, R. Sessoli, E. Krickemeyer, H. Bögge, J. Meyer, D. Gatteschi, L. Pardi, J. Westphal, K. Hovemeier, R. Rohlfing, J. Döring, F. Hellweg, C. Beugholt, M. Schmidtmann, Inorg Chem. 36 (1997) 5239.
[20] J. Livage, L. Bouhedja, C. Bonhomme, M. Henry, Mat. Res. Soc. Symp. Proc. Proc., 457 (1997) 13.
[21] Y.D. Chang, J. Salta, J. Zubieta, Angew. Chem. Int. Ed. Engl. 33 (1994) 325.

[22] W.G. Klemperer, T.A. Marquart, O.M. Yaghi, Angew. Chem. Int. Ed. Engl. 31 (1992) 49.
[23] V.W. Day, W.G. Klemperer, D.J. Maltbie, J. Am. Chem. Soc. 109 (1987) 2991.
[24] J.S. Murray, K.D. Sen (Eds.), Molecular Electrostatic Potentials, Concepts and Applications, Elsevier, Amsterdam, 1996.
[25] W.G. Klemperer, W. Shum, J. Am. Chem. Soc. 99 (1977) 3544.
[26] J.Y. Kempf, M.-M. Rohmer, J.-M. Poblet, C. Bo, M. Bénard, J. Am. Chem. Soc. 114 (1992) 1136.
[27] R.F.W. Bader, Atoms in Molecules. A Quantum Theory, Clarendon Press, Oxford, 1990.
[28] V.W. Day, W.G. Klemperer, C. Schwartz, J. Am. Chem. Soc. 109 (1987) 6030.
[29] C.J. Besecker, V.W. Day, W.G. Klemperer, M.R. Thompson, J. Am. Chem. Soc. 106 (1984) 4125.
[30] C.J. Besecker, W.G. Klemperer, J. Am. Chem. Soc. 102 (1980) 7598.
[31] V.W. Day, W.G. Klemperer, D.J. Main, Inorg. Chem. 29 (1990) 2345.
[32] W.G. Klemperer, D.J. Main, Inorg. Chem. 29 (1990) 2355.
[33] J.M. Maestre, J.P. Sarasa, C. Bo, J.M. Poblet, Inorg. Chem. 37 (1998) 3071.
[34] M.-M. Rohmer, M. Bénard, J. Am. Chem. Soc. 116 (1994) 6959.
[35] M.J. Wenninger, Polyhedron Models, Cambridge University Press, Cambridge, 1971.
[36] B.B. Karet, Z. Sun, D.D. Heinrich, J.K. McCusker, K. Folting, W.E. Streib, J.C. Huffmann, D.N. Hendrickson, G. Christou, Inorg. Chem. 35 (1996) 6450.
[37] M.-M. Rohmer, J. Devémy, R. Wiest, M. Bénard, J. Am. Chem. Soc. 118 (1996) 13007.
[38] P.S. Bagus, K. Herrmann, C.W. Bauschlicher Jr., J. Chem. Phys. 80 (1984) 4378.
[39] P.S. Bagus, K. Herrmann, C.W. Bauschlicher Jr., J. Chem. Phys. 81 (1984) 1966.
[40] N. Casañ-Pastor, L.C.W. Baker, J. Am. Chem. Soc. 114 (1992) 10384.
[41] N. Casañ-Pastor, P. Gomez-Romero, G.B. Jameson, L.C.W. Baker, J. Am. Chem. Soc. 113 (1991) 5658.
[42] J.N. Barrows, G.B. Jameson, M.T. Pope, J. Am. Chem. Soc. 107 (1985) 1771.
[43] D. Gatteschi, R. Sessoli, W. Plass, A. Müller, E. Krickemeyer, J. Meyer, D. Sölter, P. Adler, Inorg. Chem. 35 (1996) 1926.
[44] Q. Chen, C.L. Hill, Inorg. Chem. 35 (1996) 2403.
[45] E.J. Baerends, D.E. Ellis, P. Ros, Chem. Phys. 2 (1973) 41.
[46] S.H. Vosko, L. Wilk, M. Nusair, Can. J. Phys. 58 (1980) 1200.
[47] A.D. Becke, J. Chem. Phys. 84 (1986) 4524.
[48] A.D. Becke, Phys. Rev. A 38 (1988) 3098.
[49] J.P. Perdew, Phys. Rev. B 33 (1986) 8882.
[50] J.P. Perdew, Phys. Rev. B 34 (1986) 7406.
[51] M. O'Keeffe, A. Navrotsky, Structure and Bonding in Crystals, Academic Press, New York, 1981.
[52] A. Müller, M. Penk, R. Rohlfing, E. Krickemeyer, J. Döring, Angew. Chem. Int. Ed. Engl. 29 (1990) 926.
[53] Q. Chen, J. Zubieta, J. Chem. Soc., Chem. Commun. (1994) 2663.
[54] D. Riou, F. Taulelle, G. Férey, Inorg. Chem. 35 (1996) 6392.
[55] A. Müller, K. Hovemeier, R. Rohlfing, Angew. Chem. Int. Ed. Engl. 31 (1992) 1192.
[56] A. Müller, R. Rohlfing, J. Döring, M. Penk, Angew. Chem. Int. Ed. Engl. 30 (1991) 588.
[57] A. Müller, J. Mol. Struct. 325 (1994) 13.
[58] N.E. Ghermani, N. Bouhmaida, C. Lecomte, ELECTROS: computer program to calculate electrostatic properties from high-resolution X-ray diffraction. Internal Report URA CNRS 809, Université de Nancy 1, 1992.
[59] A. Müller, K. Hovemeier, E. Krickemeyer, H. Bögge, Angew. Chem. Int. Ed. Engl. 34 (1995) 779.
[60] A. Müller, S. Dillinger, E. Krickemeyer, H. Bögge, W. Plass, A. Stammler, R. Haushalter, Z. Naturforsch. B, 52 (1997) 1301.